©ESO 2022

The [CII] and FIR properties of $z > 6$ radio-loud quasars

Y. Khusanova[1], E. Bañados[1], C. Mazzucchelli[2], S. Rojas-Ruiz[1]*, E. Momjian[3], E. P. Farina[4], R. Decarli[5],
F. Walter[1], B. Venemans[6], F. Wang[7], and J. Yang[7]

[1] Max-Planck-Institut für Astronomie, Königstuhl 17, D-69117 Heidelberg, Germany
[2] European Southern Observatory, Alonso de Cordova 3107, Vitacura, Region Metropolitana, Chile
[3] National Radio Astronomy Observatory, PO Box O, Socorro, NM 87801, USA
[4] Gemini Observatory, NSF's NOIRLab, 670 N A'ohoku Place, Hilo, Hawai'i 96720, USA
[5] INAF - Osservatorio di Astrofisica e Scienza dello Spazio di Bologna, via Gobetti 93/3, I-40129, Bologna, Italy
[6] Leiden Observatory, Leiden University, PO Box 9513, 2300 RA Leiden, The Netherlands
[7] Steward Observatory, University of Arizona, 933 N. Cherry Ave., Tucson, AZ 85721, USA

March 27, 2022

ABSTRACT

There are only five radio-loud quasars currently known within 1 Gyr from the Big Bang ($z > 6$) and the properties of their host galaxies have not been explored in detail. We present a NOrthern Extended Millimeter Array (NOEMA) survey of [CII] (158 μm) and underlying continuum emission of four $z > 6$ radio-loud quasars, revealing their diverse properties. J0309+2717 ($z = 6.10$) has a bright [CII] line and underlying continuum, implying a starburst with a star-formation rate SFR=340–1200 $M_\odot$ yr^{-1}. J1429+5447 ($z = 6.18$) has a SFR=$520 - 870$ $M_\odot$yr^{-1} and its [CII] profile is consistent with two Gaussians, which could be interpreted as a galaxy merger. J1427+3312 ($z = 6.12$) has a moderate SFR = 30–90 $M_\odot$ yr^{-1}. Notably, this is a broad absorption line quasar and we searched for the presence of high-velocity outflows in the host galaxy. Although the NOEMA data revea a tentative broad component of the [CII] line as wide as ~1400 km s^{-1}, the sensitivity of our current data is not sufficient to confirm it. Finally, P172+18 ($z = 6.82$) is undetected in both [CII] and continuum, implying a SFR< $22 - 40$ $M_\odot$yr^{-1}. The broad range of SFRs is similar to what is observed in radio-quiet quasars at similar redshifts. If radio jets do not significantly contribute to both [CII] and IR luminosities, this suggest no feedback from the jet on the star formation in the host galaxy.

1. Introduction

The formation and evolution of supermassive black holes is one of the key unresolved puzzles in astrophysics. Black holes (BHs) of masses $\sim 10^9 M_\odot$ are already in place in the first Gyr after the Big Bang (e.g., Bañados et al. 2018b; Yang et al. 2020; Wang et al. 2021). It is still a mystery how these BHs acquire such masses and how their evolution is connected to that of the host galaxies (e.g., Inayoshi et al. 2020; Volonteri et al. 2021). The mergers of host galaxies can lead to a coalescence of their respective BHs, while simultaneously playing a role in driving the gas towards the center, thus enabling efficient accretion onto the BH. This can result in the formation of relativistic jets (e.g. Chiaberge et al. 2015). The presence of a jet allows to partially convert accretion power to non-radiative form, thus enhancing the accretion rate (e.g., Jolley & Kuncic 2008). Hence, mergers of host galaxies and possible subsequent formation of jets can play a crucial role in the fast growth of BHs in the early Universe (Volonteri et al. 2015).

The presence of jets can affect the evolution of the host galaxies in different ways. While AGN-driven extreme gas outflows can lead to quenching of star formation in the host galaxy (e.g., Di Matteo et al. 2005; Villar Martín et al. 2014), these jets can also trigger enhanced star formation in the host galaxy via AGN-induced pressure (e.g., Silk 2013). It is unclear which mechanism plays the most im-

portant role at high redshift, since no systematic study of host galaxies of quasars with jets at $z \gtrsim 6$ has been undertaken. Relativistic jets produce synchrotron radio emission. Therefore, radio-loudness[1] $R_{4400} > 10$ is a sign of the existence of such jets. Such quasars are considered radio-loud and quasars with $R_{4400} < 10$ are called radio-quiet.

The host galaxies of radio-quiet quasars at $z \gtrsim 6$ have been extensively observed using the Atacama Large Millimeter/submillimeter Array (ALMA) and the NOrthern Extended Millimeter Array (NOEMA) revealing the cold dust emission in the rest-frame far-infrared (FIR) and [CII] line emission (e.g. Wang et al. 2013; Willott et al. 2015; Bañados et al. 2015a; Willott et al. 2017; Decarli et al. 2018; Izumi et al. 2018, 2019; Venemans et al. 2020). These studies showed that the host galaxies of radio-quiet quasars have star formation rates (SFRs) reaching up to 2500 M$_\odot$/yr (e.g., Venemans et al. 2020) and one third shows signs of recent mergers (Neeleman et al. 2021). Many studies have sought out to confirm active galactic nuclei (AGN) driven outflows in the host galaxies. However, the results are still inconclusive (Cicone et al. 2015; Bischetti et al. 2019; Novak et al. 2020; Meyer et al. 2022). Moreover, it is unknown whether the host galaxies of radio-loud quasars differ from those of radio-quiet ones, whether they have outflows, how common are mergers among them and how the radio-mode AGN feedback affects star formation at $z > 6$.

---

[1] $R_{4400} = S_{5GHz}/S_{4400Å}$, where S_{5GHz} and S_{4400} are flux densities at the rest-frame at 5 GHz and 4400 Å, respectively (Kellermann et al. 1989)

Radio-loud quasars are relatively rare as they constitute only 8-10% of quasar population at $z \gtrsim 6$ (Bañados et al. 2015b; Liu et al. 2021; Gloudemans et al. 2021). To date there are only five radio-loud quasars known at $z > 6$: J1427+3312 at $z = 6.12$ (McGreer et al. 2006), J1429+5447 at $z = 6.18$ (Willott et al. 2010), J0309+2717 at $z = 6.10$ (Belladitta et al. 2020), J2318–3113 at $z = 6.44$ (Ighina et al. 2021) and P172+18 at $z = 6.83$ (Bañados et al. 2021). Only the rest-frame FIR properties of one of them, J2318–3113, have been studied before this source was recognized as radio-loud (Decarli et al. 2018; Venemans et al. 2020; Neeleman et al. 2021).

In this paper, we report NOEMA observations of [CII] emission and the underlying continuum for the remaining 4 radio-loud quasars known at $z > 6$. In Section 2, we describe the observations and data reduction. In Section 3, we present the results for individual objects and discuss their properties. In Section 4, we compare the [CII] emission and dust properties of all currently known $z \gtrsim 6$ radio-loud quasars with the samples of radio-quiet quasars at $z \gtrsim 6$ from the literature. Finally, in Section 5 we present our conclusions. Throughout the paper we use ΛCDM cosmology with $\Omega_\Lambda = 0.70$, $\Omega_m = 0.30$ and $h = H_0/100 = 0.7$.

2. Data

We have observed four out of the five known $z > 6$ radio-loud quasars with NOEMA. J1427+3312, J1429+5447 and P172+18 were observed in 2019, December 3rd, June 16th and August 14th, as part of the S19DN observing programme. J0309+2717 was observed in 2020, June 18th, 20th and July 20th as part of the S20CY observing programme. All targets were observed in band 3, which covers the range $\sim 208 - 264$ GHz range where the redshifted [CII] emission line ($\nu_{\rm rest} = 1900.539$ GHz) falls at $z \gtrsim 6$. The tuning frequencies were chosen so that the [CII] emission falls in one of the side bands. The other side band can be used for FIR continuum emission measurements.

The observations were carried out using configurations C, D or a combination of the two. Configuration D is the most compact and provides angular resolution $\sim 1\rlap{.}''5$ (~ 8 kpc). Configuration C is more extended and provides resolution $\sim 0\rlap{.}''8$ (~ 4 kpc). Most observations were carried out with 10 antennas, except for J1429+5447 and one of the tracks for J1427+3312, for which 9 antennas were used. The beam sizes (0.5–1.7 arcsec) correspond to 3–10 kpc at the quasar redshifts. The total integration time, configuration used, and synthesized beam for each quasar are listed in Table 1.

The data were calibrated using the standard calibration steps in the GILDAS software[2]. We used 3C84, 3C345, 3C273 or 3C279 sources for bandpass calibration. The phase and amplitude were calibrated using 1417+273, 1418+546, 1147+245. The flux density scale was calibrated using LKHA101 for P172+18 and MWC349 for the rest of the sample. We flagged bad visibilities before producing the *uv* tables. We resampled all *uv* tables to the resolution of 50 km s^{-1}.

The dirty images were produced from the *uv* tables using *MAPPING* software package (part of GILDAS). We used natural weighting, since we expect that our targets will not be resolved and they are exactly at the center of the

image where natural weighting yields the optimal sensitivity. The clean images were produced using the HOGBOM method (Högbom 1974) in *MAPPING*.

We produced continuum maps using the [CII] emission-free side band by averaging all the channels in this band. Before producing [CII] emission line maps, we averaged all the channels in the side band containing the [CII] emission to produce preliminary images. We found $>3\sigma$ detections in the center of the images of J1427+3312, J1429+5447 and J0309+2717. We then extracted spectra from the brightest pixel in this image to search for the [CII] emission line. Since no significant emission was found on the preliminary image of P172+18, we extracted spectra from the central pixel that is located at the optical position of the quasar (Bañados et al. 2021). We used the publicly available code Interferopy (Boogaard, Meyer, & Novak 2021) to measure the flux densities using the residual scaling correction (Jorsater & van Moorsel 1995; Walter & Brinks 1999; Novak et al. 2020). In this method, the flux density measured on the clean components map is corrected by the scaled residual flux density. The scaling factor is defined as the clean-to-dirty beam area ratio. This ensures consistency between the units of the residual flux (in Jy/dirty beam) and the clean components (in Jy/clean beam). We found $>3\sigma$ [CII] line detections for all targets where emission was detected on a preliminary image. We fit all the [CII] emission line profiles detected with a single Gaussian. We estimated the continuum emission excluding all the channels within ±1000 km s^{-1} from the peak of the [CII] line. We subtracted the continuum using the task *UV_BASELINE* in *MAPPING*. We then produced integrated [CII] line maps using channels containing the line across 1.2×FWHM (in case of a non-detection, we used FWHM=350 km s^{-1}).

Using the [CII] line maps, we determine the optimal aperture radius to extract the spectra by performing a curve-of-growth analysis. We start with an aperture size equal to the half of the semi-major axis of the beam (this is also the aperture size which we used in case of a non-detection). We chose the aperture radius at which increasing the radius changes the measured aperture integrated flux density only within 1σ. In this way, we make sure that we do not miss any flux of an unresolved source and do not introduce additional noise if we chose a bigger aperture. Similarly, we chose the aperture for measuring the continuum flux density.

3. Results

Our analysis reveals a range of host galaxy properties of radio-loud quasars. The [CII] line and underlying continuum were detected for J1427+3312, J1429+5447, J0309+2717, while they were not detected for P172+18. The [CII] and underlying continuum emission line measurement results are summarized in Table 2. Fig. 1 shows the 250 GHz continuum and [CII] line maps and the spectra zoomed on the [CII] emission line. Below we discuss the results for each individual object in the sample ordered by their redshift.

3.1. J0309+2717 ($z = 6.10$)

J0309+2717 is the most radio-loud quasar at $z > 6$. Based on its radio and X-ray properties, this source was classified

---

[2] https://www.iram.fr/IRAMFR/GILDAS

Table 1. NOEMA observations

Quasar	R_{4400}[a]	Integration time (hours)	Configuration	Beam size (arcsec)
J0309+2717	2500 ± 500[b]	4.8	D	1.7×1.1
J1427+3312	53.3 ± 4.1[c]	3.4	CD	1.1×0.7
J1429+5447	109.2 ± 4.1[c]	3.4	D	1.6×1.4
P172+18	70 ± 7[d]	4.1	C	1.1×0.5

Notes. [a] Radio-loudness $R_{4400} = S_{5GHz}/S_{4400Å}$ (Kellermann et al. 1989). [b] Belladitta et al. (2020) [c] Bañados et al. (2015b) [d] Bañados et al. (2021)

Table 2. [CII] and underlying continuum emission measurements of the sample presented in this paper and from the radio-loud quasars at $z \gtrsim 6$ in the literature

Quasar	$z_{[CII]}$	F_{cont} (mJy)	$F_{[CII]}$ (Jy km s^{-1})	FWHM (km s^{-1})
J0309+2717	6.100 ± 0.002	4.39 ± 0.15	2.6 ± 0.2	240 ± 20
J1427+3312	6.118 ± 0.006	0.18 ± 0.05	0.7 ± 0.1	440 ± 69
J1429+5447	6.190 ± 0.004	3.05 ± 0.11	3.6 ± 0.2	359 ± 24
P172+18	$6.823^{+0.003}_{-0.001}$[a]	<0.34[b]	<0.21[b]	$-$
J2318-3113[c]	6.4429 ± 0.0003	0.36 ± 0.08	1.52 ± 0.14	344 ± 34
P352-15[d]	5.832 ± 0.001	0.34 ± 0.04	1.37 ± 0.22	440 ± 80

Notes. [a] This redshift is measured based on MgII emission line (Bañados et al. 2021). [b] The limits are at 3σ and assuming FWHM=350 km s^{-1}. [c] The measurements are taken from Venemans et al. (2020) [d] The measurements are taken from Rojas-Ruiz et al. (2021)

as a blazar and currently it is the only blazar at $z > 6$ (Belladitta et al. 2020). A one-sided jet launched by this quasar is pointing towards an observer at the angle smaller than 38° based on high resolution observations with the Karl G. Jansky Very Large Array (VLA) of the National Radio Astronomy Observatory (NRAO, Spingola et al. 2020). The jet is seen in X-ray and is extended across $\sim 4''$ or ~ 20 kpc (Ighina et al. 2022). The radio spectrum of J0309+2717 is flat with a spectral index $\alpha = -0.53 \pm 0.02$ at frequencies from 0.147 GHz to 8.2 GHz (see Fig. 3, Ighina et al. 2022; Mufakharov et al. 2020).

J0309+2717 has the brightest 250 GHz continuum emission in our sample ($F_{cont} = 4.39 \pm 0.15$ mJy) and the second brightest [CII] line emission ($F_{[CII]} = 2.6 \pm 0.2$ Jy km s^{-1}). The source is unresolved. No significance difference in shape is observed between the spectrum extracted from the brightest pixel and from an aperture with $3.4''$ diameter (see Fig. 1). But the spectra extracted with an aperture has a higher flux density (by a factor of ~ 1.2), since some of the flux is missed if a single pixel is used to extract the spectrum. Therefore, we use the aperture extracted spectrum in further analysis in Section 4.

3.2. J1427+3312 ($z = 6.12$)

J1427+3312 is the first radio-loud quasar discovered at $z > 6$ (McGreer et al. 2006). After the discovery, two independent Very Long Baseline Interferometry (VLBI) follow-up studies of J1427+3312 were conducted. Momjian et al. (2008) observed a structure with two continuum components at 1.4 GHz, separated by 176 pc. Frey et al. (2008) observed J1427+3312 at 1.6 and 5 GHz and the 1.6 GHz observations revealed a double structure of this quasar with two components separated by 160 pc, comparable to the separation observed by Momjian et al. (2008). Both these studies conclude that these two components could be the ra-

dio lobes and J1427+3312 could be a Compact Symmetric Object (CSO, Conway 2002) with a steep radio spectrum ($\alpha = -1.1$). Based on its rest-frame ultraviolet (UV) spectrum, this source was also classified as a Broad Absorption Line (BAL) quasar (McGreer et al. 2006; Shen et al. 2019).

Our NOEMA observations reveal a [CII] line emission with $F_{[CII],int} = 0.7 \pm 0.1$ Jy km s^{-1}. The curve of growth analysis shows that even with the small aperture the noise in the spectrum significantly increases compared to the extraction from a single pixel since the source is unresolved. We use, therefore, the spectrum extracted from the brightest pixel in the analysis in Section 4. We use the fit with a Gaussian to this spectrum to select the channels containing the line. On the integrated image (including only the channels across 1.2×FWHM), the [CII] emission is detected with a 4σ significance. In the channel corresponding to the peak of the line, the significance of the line is 8σ. The emission is unresolved at the resolution of our observations. The 250 GHz continuum has a flux density $F_{cont} = 0.18 \pm 0.05$ mJy.

3.3. J1429+5447 ($z = 6.19$)

J1429+5447 is one of the most studied in the literature objects in our sample. Radio observations of J1429+5447 cover the range from 120 MHz to 1.6 GHz (see Fig. 3, Frey et al. 2011; Shimwell et al. 2019). The radio spectrum is flat at frequencies < 5 GHz (spectral index $\alpha \sim 0.5$) but steepends at higher frequencies (spectral index $\alpha = -1.0$, Frey et al. 2011). The high resolution VLBI observations of this quasar show a compact structure with a size <100 pc. It was also observed at 32 GHz (Wang et al. 2011). These observations targeted CO (2–1) emission line and they tentatively suggest the presence of a companion galaxy separated by 6.9 kpc. J1429+5447 was also observed with eROSITA and
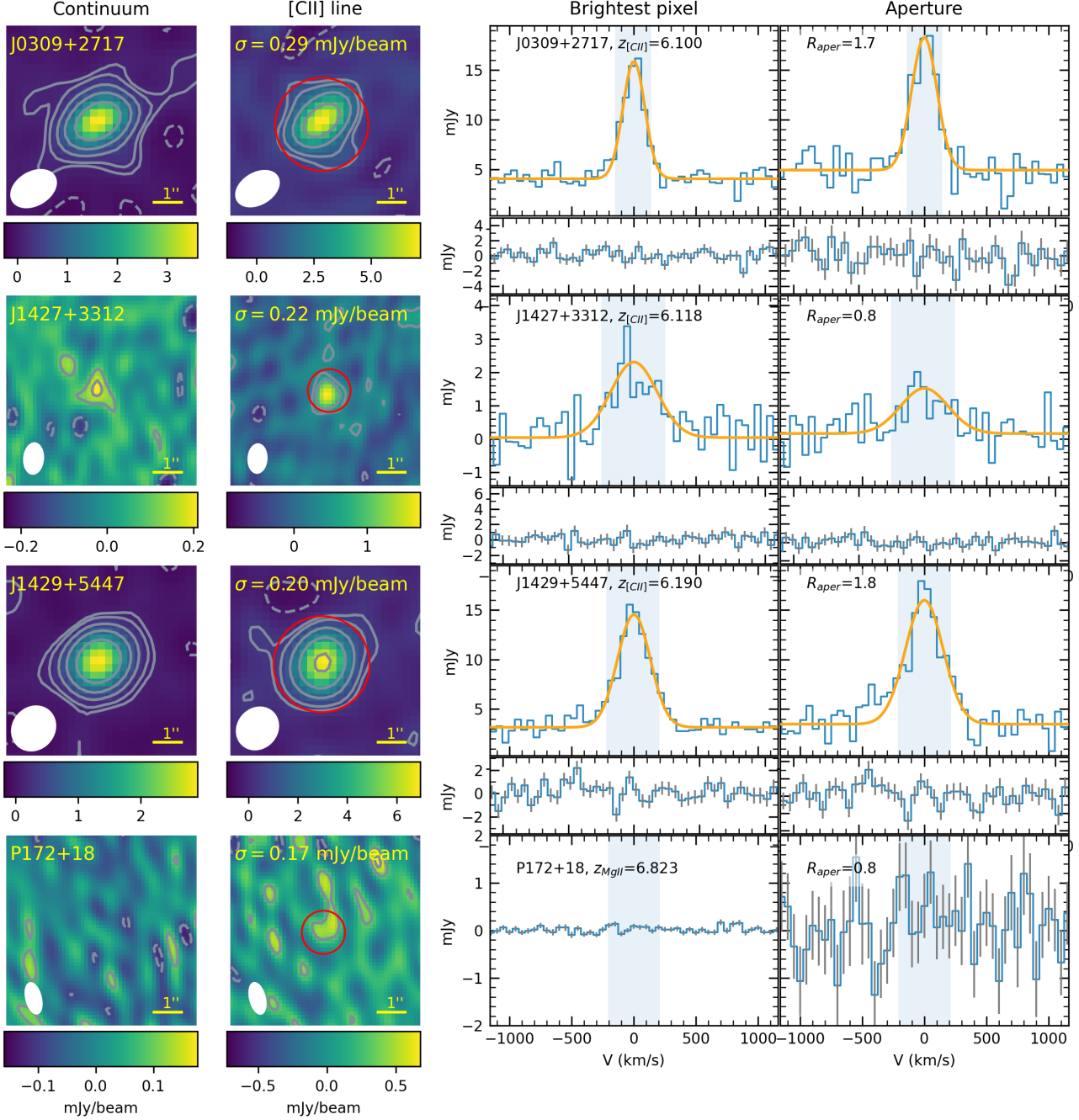
Fig. 1. The images and spectra of the radio-loud quasars in our sample. First column: the 250 GHz continuum images. The contour levels are (-2, 2, 3.5, 8, 16, 32)×σ where $\sigma = 0.05$ mJy/beam. Second column: The integrated [CII] line images (continuum subtracted). The contour levels are (-2, 2, 3.5, 8, 16, 32)×σ and σ values are shown on images. The contour levels are the same as in the first column. The red circles show the apertures, from which the spectrum in the fourth column was extracted. Third column: Spectra from the brightest (central) pixel. The solid orange line shows the best fit to the line with a Gaussian. The shaded area shows the channels used to create the integrated maps on the second column. Fourth column: spectra extracted using the apertures shown in images in the second column (see Section 2).

XMM-Newton and currently it is the brightest X-ray source at $z > 6$ (Medvedev et al. 2020, 2021).

J1429+5447 is the second brightest quasar in our sample at ~250 GHz ($F_{cont} = 3.05 \pm 0.11$ mJy) and has the brightest [CII] emission line ($F_{[CII],int} = 3.6 \pm 0.2$ Jy km s^{-1}). Interestingly, when we extract the spectrum with an aperture, thus accounting for all the flux seen in the [CII] line

image, additional flux deviant from a single Gaussian profile appears. This may indicate that J1429+5447 is hosted in merging galaxies or that its host has AGN-driven outflows. We will discuss this in more detail in Section 4.1.

3.4. P172+18 ($z = 6.82$)

P172+18 is the highest redshift quasar in our sample and the highest redshift radio-loud quasar known to date (Bañados et al. 2021). The radio spectrum of P172+18 is steep with a spectral index $\alpha < -1.55$ (see Fig. 3, Momjian et al. 2021). It suggests that P172+18 is a Gigahertz Peaked Source (GSP). It is the only source from our sample, which is not detected in both [CII] and continuum emission (see Fig. 1). The 3σ upper limit for the FIR continuum flux density is $F_{cont} < 0.34$ mJy. We determine the upper limit for the [CII] flux density assuming the mean FWHM of the [CII] emission line in the host galaxies of radio-quiet quasars at $z > 6$ FWHM=350 km s^{-1} (Decarli et al. 2018; Venemans et al. 2020). The 3σ upper limit with this assumption is $F_{[CII],int} < 0.21$ Jy km s^{-1}.

4. Discussion

4.1. Are host galaxies of radio-loud quasars mergers or outflows?

At redshifts $1 < z < 2.5$, 92% of radio-loud quasars are hosted in merging galaxies compared to 38% of radio-quiet quasars (Chiaberge et al. 2015). The merger fraction of radio-quiet quasars at $z \gtrsim 6$ is $\sim 29\%$[3] (Neeleman et al. 2021). This suggests no evolution with redshift of the merger fraction in radio-quiet quasars. Assuming that the merger fraction in radio-loud quasars does not evolve either, most host galaxies of radio-loud quasars at $z \gtrsim 6$ should be mergers. The recently identified a $z = 6.44$ radio-loud quasar J2318–3113 (Ighina et al. 2021) whose kinematics and morphology were studied in detail by Neeleman et al. (2021) using observations with ALMA at high spatial resolution (~ 1 kpc). They find that J2318–3113 has a disturbed morphology indicative of a recent or ongoing merger activity (see Fig. 2 in Neeleman et al. 2021). The spatial resolution of our NOEMA data (~ 6 kpc) is not sufficient to perform such analysis. Therefore, we focus on analysing the spectral shape of the [CII] line in order to search for signs of mergers.

We noted in Section 3 that the [CII] spectrum of J1429+5447 shows a broader component when extracted with an aperture ($R = 1''77$) We fit this spectrum with two Gaussians. The two components have redshifts $z_{broad} = 6.19 \pm 0.009$ and $z_{narrow} = 6.19 \pm 0.003$ and FWHM$_{broad} = 650 \pm 128$ km s^{-1} and FWHM$_{narrow} = 253 \pm 38$ km s^{-1}. The fit with two components is preferred by both Akaike Information Criterion (AIC) and Bayesian Information Criterion (BIC, the values are listed in Table 3), although the BIC difference does not exceed the threshold $\Delta BIC > 10$ for a strong significance (Kass & Raftery 1995). The χ^2 difference implies p-value of $p = 0.99996$ for three additional degrees of freedom or 3.95σ significance for a broad component.

Previously, the CO (2–1) emission of J1429+5447 was observed with a resolution of ~ 0.7 arcsec at 32 GHz with the VLA. Wang et al. (2011) report the presence of two components of CO (2–1) emission line where the broad

component is detected at 4σ significance. The two components have redshifts $z_{east} = 6.1837$ and FWHM$_{east} = 400$ km s^{-1}, and $z_{west} = 6.1831$ and FWHM$_{west} = 280$ km s^{-1}. The widths and redshifts of the CO (2–1) line are consistent with the ones we obtained from the best fit of the [CII] line profile on the spectrum from the aperture. The similarity of the widths of the spectral profiles of the CO(2–1) and [CII] lines suggests that the [CII] emission arises from the same structure as the reported CO (2–1) emission. In that case, J1429+5447 is likely to be a merger or two gravitationally interacting sources.

We cannot completely separate the narrow component from the broad one, but by averaging the channels within $1.2 \times$ FWHM of the broad component and excluding all the channels across $1.2 \times$ FWHM of the narrow component, we can obtain an image with little contamination from a narrow component. In order to obtain an image of the narrow component, we average the channels across $1.2 \times$ FWHM$_{narrow}$. These channels still contain emission from the broad component, but the emission from the narrow component is comparable to the broad one or dominates it. We show the images for the narrow and broad components in Fig. 2. The [CII] emitting regions of the broad and narrow component still overlap and we cannot make firm conclusions whether they could be separated as the CO(2–1) line emission observed by Wang et al. (2011). The size of the NOEMA beam is 1.6×1.4 arcsec, almost two times larger than the beam of the CO(2–1) line observations and larger than the separation between the components on the CO(2–1) line map. Therefore, higher angular resolution [CII] observations are necessary to make firm conclusions about the nature of the broad and narrow [CII] emission in this system.

We performed a similar analysis for the remaining quasars with a [CII] detection in our sample. J0309+2717 has no indication of a second component. The fit with two Gaussians results in adding a negative broad Gaussian shifted by more than 1000 km s^{-1} from the [CII] line center. This broad component does not have a physical meaning and is discarded by the BIC. The difference in AIC is not significant (see Table 3). We conclude that the spectrum of J0309+2717 is represented by one Gaussian.

In Section 3, we noted that J1429+3312 is unresolved and extracting the spectrum with an aperture results in a lower signal to noise ratio (SNR). Therefore, we test the fit with one and two Gaussians on the spectrum extracted from the brightest pixel. The fit with two Gaussians reveals a broad component of [CII] emission with FWHM$_{broad} \sim 1400$ km s^{-1}. The narrow component has FWHM$_{narrow} = 343 \pm 113$ km s^{-1} consistent with the width of the fit with a single Gaussian. The width of the broad component is consistent with what is expected for outflows.

The existence of the outflows in host galaxies of radio-quiet quasars is debated in the literature. Individual radio-quiet quasars observed at $\nu_{rest} \sim 1900$ GHz predominantly have single Gaussian profiles of [CII] line with FWHM$_{[CII]} \sim 350$ km s^{-1} (Decarli et al. 2018; Novak et al. 2020). Maiolino et al. (2012) and Cicone et al. (2015) found such outflows in the host galaxy of J1148+5251, but later observations of this object by Meyer et al. (2022) with a larger number of antennas and the new wide-band correlator PolyFiX of NOEMA did not confirm the presence of a [CII] outflow in the host galaxy. Decarli et al. (2018) approached the search for outflows using the stacking of

---

[3] This value is calculated considering only the quasars which are confirmed to be radio-quiet. Including the quasars whose radio-loudness is unknown results in merger fraction 31%. Taking into account that $\sim 10\%$ of them could be radio-loud, the upper limit of the merger fraction of radio-quiet quasars is $\sim 39\%$.

Table 3. The statistical criteria values for selection between the fit with one Gaussian and two Gaussians.

Quasar	$\Delta\chi^2$	p-value	$\Delta\mathrm{AIC}^a$	$\Delta\mathrm{BIC}^a$
J0309+2717	4.99	0.82738	0.47	-10.83
J1427+3312	0.92	0.17997	-3.82	-10.93
J1429+5447	23.08	0.99996	10.02	2.91

Notes. $^{(a)}$ $\Delta\mathrm{AIC}$, $\Delta\mathrm{BIC} < -10$ imply that the fit with one Gaussian is preferred. $\Delta\mathrm{AIC}$, $\Delta\mathrm{BIC} > 10$ imply that two Gaussians are preferred.
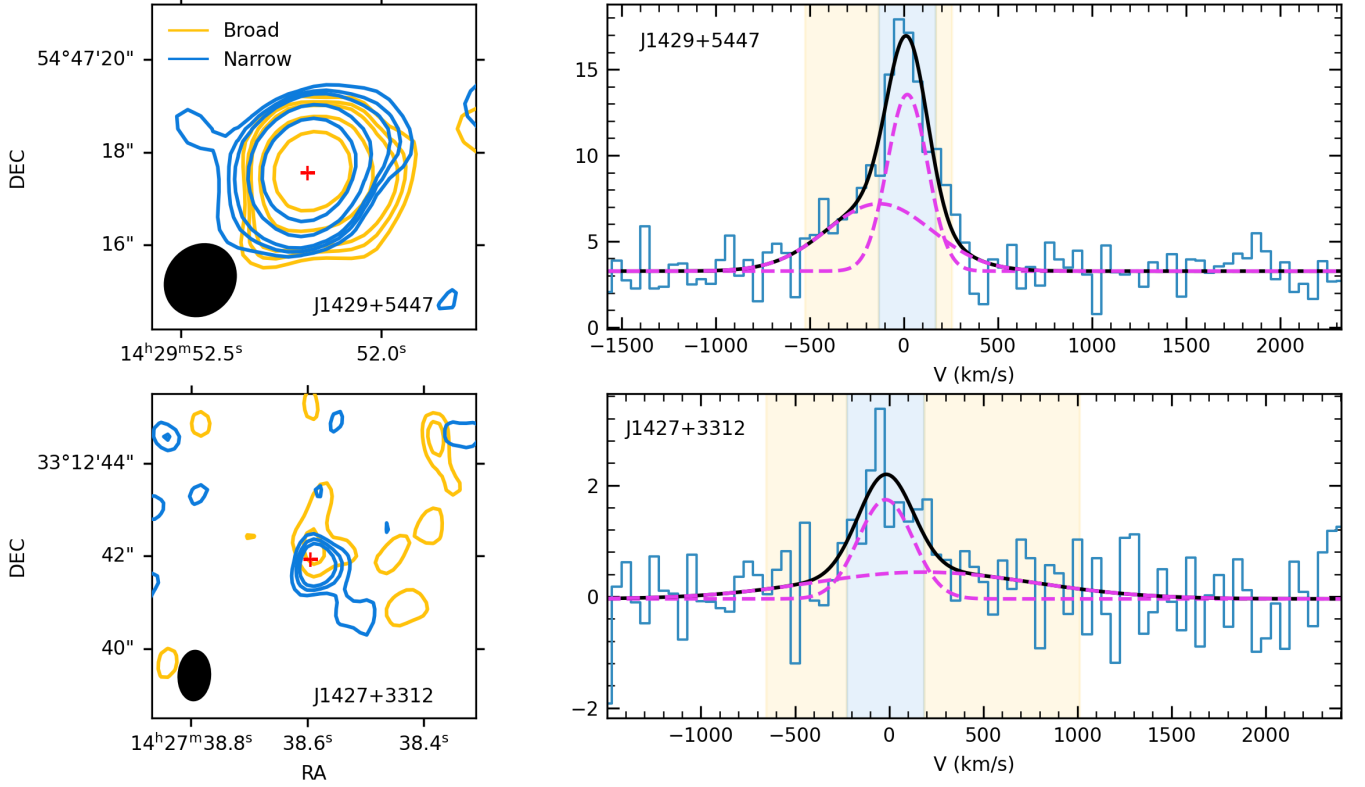
Fig. 2. The images of the broad and narrow components and the spectra of J1429+5447 (*top*) and J1427+3312 (*bottom*). First column: the contours on the images (blue for the narrow and yellow for the broad component). The contours correspond to $(2,3,4,8,16)\times\sigma$. Second column: the spectra (blue line) and the fit with two Gaussians (black solid line). The magenta dashed lines are broad and narrow components of the fit with two Gaussians. The shaded areas shows the channels used to produce corresponding images of the broad and narrow components.

ALMA [CII] observations and did not find outflow signatures. On the contrary, Bischetti et al. (2019) reports an evidence of a weak broad component with $\mathrm{FWHM}_{[CII]}^{broad} = 1730\pm210$ km s^{-1} in the stacked spectrum. However, this is a delicate issue that might depend on different techniques employed. Novak et al. (2020) used the stacking in the *uv*-plane instead of the image plane and did not find any indication for a presence of the broad component. While the spectral profile of J1429+5447 has indication of a narrow and a broad component, the width of the broad component is much smaller than what is typical for the outflows (i.e., a few 1000s km s^{-1}).

J1427+3312 was previously classified as BAL quasar (McGreer et al. 2006; Shen et al. 2019). Hence, the host galaxy of this quasar can have high-velocity outflows. We separate the broad and narrow component of J1427+3312 in the same way as described above for J1429+5447 and show the results in Fig. 2. The broad component only has

a 3σ emission close to the optical position of the quasar. The fit with two Gaussians, however, is discarded by BIC (see Table 3). The AIC neither discards nor confirms the presence of the second Gaussian. As an additional test, we compared the fit with one and two Gaussians to the spectrum extracted with an aperture. The broad component with the width compatible with an outflow scenario ($\mathrm{FWHM}_{broad} \sim 940$ km s^{-1}) appears in the fit with two Gaussians to this spectrum as well. Both the BIC and AIC for that fit neither discard nor confirm the broad component. Since the [CII] emission line of J1427+3312 is rather faint and the SNR is low with the sensitivity of our observations, the presence of high-velocity outflows in J1427+3312 requires further investigation with higher sensitivity follow-up observations.
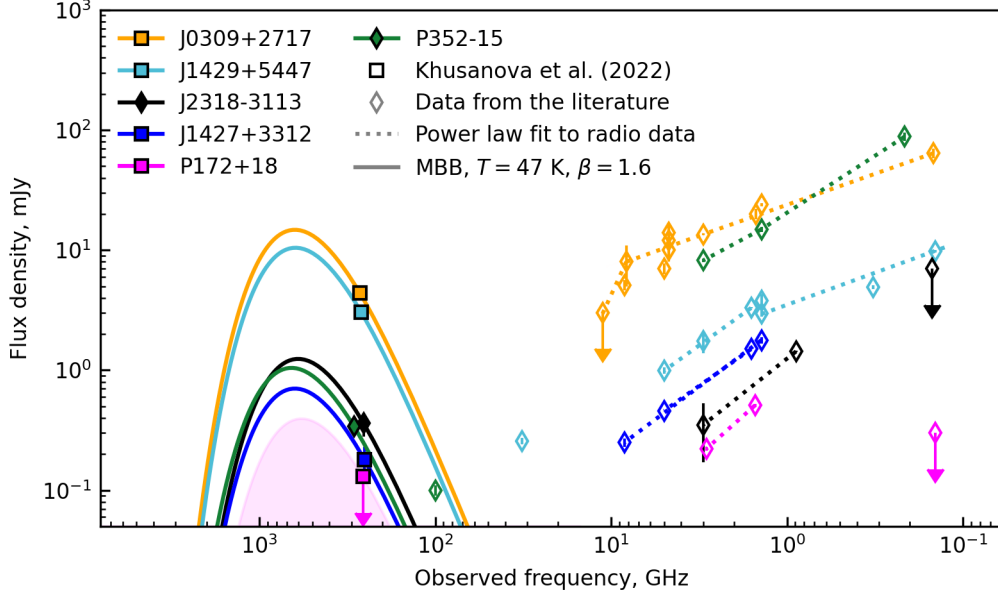
Fig. 3. SEDs of all known radio-loud quasars at $z > 6$ and P352–15 at $z = 5.832$. The filled symbols are measurements of the 250 GHz continuum flux density (NOEMA measurements presented in this paper and literature data from ALMA for J2318-3113 Venemans et al. 2020). The solid lines are MBB model (with $T_{dust} = 47$ and $\beta = 1.6$) scaled to the observed continuum flux density. The dotted lines are the power law (broken power law in the case of J0309+2717 and J1429+5447) fits to the radio data from the literature (Bañados et al. 2021; Condon et al. 1998; Frey et al. 2008, 2011; Ighina et al. 2021; Intema et al. 2017; Momjian et al. 2008; Shimwell et al. 2019; Wang et al. 2011). The literature data are shown with thin diamonds and the NOEMA data for our sample with squares. Different colors correspond to each of the radio-loud quasars as indicated in the legend. The shaded area shows the region below the 3σ limit for continuum flux density of P172+18, which is not detected with NOEMA.

4.2. The effects of the jet on star formation

The presence of radio-jets can enhance as well as quench star formation in the host galaxy. Mandal et al. (2021) suggest that both effects are present with increased SFR closer to the center of the host galaxy and decreased SFR on the outskirts. The IR and [CII] observations have been extensively used to estimate SFRs of host galaxies of radio-quiet quasars (e.g. Decarli et al. 2018; Venemans et al. 2020). Their SFRs reach up to $\sim$2500 M$_\odot$/yr with a median of the SFR distribution at $\sim$250 M$_\odot$/yr. Here we compare these results with our measurements for the host galaxies of $z \gtrsim 6$ radio-loud quasars.

To determine the IR luminosities, we use the modified black body model (MBB) and optically thin approximation (Beelen et al. 2006):

$$S_{\nu_{obs}} = f_{CMB} \frac{1+z}{D_L^2} \kappa_d(\nu_{rest}, \beta) \frac{2h\nu_{rest}^3}{c^2} \frac{M_{dust}}{e^{h\nu_{rest}/k_b T_{dust,z}} - 1}, \quad (1)$$

where f_{CMB} is a correction for the Cosmic Microwave Background (CMB) contrast, D_L is the luminosity distance, $\kappa_d(\nu_{rest}, \beta) = \kappa_{d(\nu_0)}(\nu_{rest}/\nu_o)^\beta$ cm^{2}g^{-1} is the opacity law, M_{dust} is the dust mass, $T_{dust,z}$ is the dust temperature at given redshift, β is the emissivity index and $\nu_{rest} = (1 + z)\nu_{obs}$ is the rest frame frequency. For the opacity law, we assume values $\kappa_{d(\nu_0)} = 2.64$ m^{2}kg^{-1} at $\nu_0 = c/(125\mu m)$ from Dunne et al. (2003). The dust temperature heated by the CMB is:

$$T_{dust,z} = (T_{dust}^{\beta+4} + T_{CMB,z=0}^{\beta+4}[(1+z)^{\beta+4} - 1])^{\frac{1}{\beta+4}}, \quad (2)$$

where T_{dust} is the intrinsic dust temperature and $T_{CMB,z=0}$ is the CMB temperature at $z = 0$ (da Cunha et al. 2013). Here, we assume $T_{dust} = 47$ K and the emissivity index $\beta = 1.6$ (Beelen et al. 2006). The CMB contrast is defined as:

$$f_{CMB} = 1 - \frac{B_{\nu_{rest}}(T_{CMB,z})}{B_{\nu_{rest}}(T_{dust,z})} \quad (3)$$

where $T_{CMB,z}$ is the CMB temperature at redshift z and $B_{\nu_{rest}}$ is the black body radiation spectrum. We scale the MBB to the continuum flux density at $\nu_{rest} \sim 1900$ GHz and obtain the IR luminosity by integrating between 8 μm and 1000 μm (see Fig. 3). We convert the IR luminosity to SFR using the Kennicutt (1998) relation:

$$SFR_{IR} = \kappa_{IR}L_{IR}, \quad (4)$$

where L_{IR} is the IR luminosity and $\kappa_{IR} = 10^{-10}M_\odot\text{yr}^{-1}L_\odot^{-1}$ is a conversion factor assuming Chabrier (2003) initial mass function.

We use the De Looze et al. (2014) relation to convert [CII] luminosities to SFRs:

$$\frac{SFR_{[CII]}}{M_\odot yr^{-1}} = 3 \times 10^{-9} \left(\frac{L_{[CII]}}{L_\odot}\right)^{1.18}. \quad (5)$$

The [CII] luminosity is calculated as

$$\frac{L_{[CII]}}{L_\odot} = 1.04 \times 10^{-3} \frac{F_{[CII]}}{\text{Jy km s}^{-1}} \frac{\nu_{obs}}{\text{GHz}} \left(\frac{D_L}{\text{Mpc}}\right)^2 . \qquad (6)$$

where $F_{[CII]}$ are the [CII] line fluxes, ν_{obs} is the observed frequency of the [CII] line and D_L is the luminosity distance (e.g., Carilli & Walter 2013).

Following this approach, we calculated [CII] and IR luminosities of all radio-loud quasars at $z > 6$ and P352–15 at $z = 5.832$ (Rojas-Ruiz et al. 2021). We use the data from the literature for J2318–3113 and P352–15, which were previously observed with ALMA(Venemans et al. 2020; Rojas-Ruiz et al. 2021). The results are summarized in Table 4. In Fig. 4, we also show the SFRs of the radio-quiet quasars, for which we used as input the observed flux densities reported in the literature (Andika et al. 2020; Bañados et al. 2015a; Decarli et al. 2017, 2018; Eilers et al. 2020; Izumi et al. 2018, 2019; Maiolino et al. 2005; Venemans et al. 2012, 2016, 2017, 2020; Walter et al. 2009; Wang et al. 2013, 2016, 2021; Willott et al. 2013, 2015, 2017; Yang et al. 2019, 2020). We then followed a consistent approach to derive their luminosities and SFRs as described above.

The SFR_{IR} agrees well with the $\text{SFR}_{[CII]}$ with a scatter of ~ 0.3 dex around the 1-to-1 relation for both radio-quiet and radio-loud quasars. The [CII] luminosities and $\text{SFR}_{[CII]}$ of the radio-loud quasars are in good agreement with the distribution for radio-quiet quasars. This is, however, not the case for IR luminosities and SFR_{IR}. The faintest radio-loud quasars fall all below the 21st percentile of the distribution of radio-quiet quasars, while the brightest are above $\sim$81st percentile. No radio-loud quasar falls within 0.65σ from the median of the SFR_{IR} distribution of radio-quiet quasars. This could be an indication of a bimodal distribution of IR luminosities of radio-loud quasars or simply a result of a small number statistics.

We use two sample Kolmogorov-Smirnov (KS) test to determine, whether the SFRs of radio-quiet and radio-loud quasars come from the same distribution. For $\text{SFR}_{[CII]}$, the KS statistic is 0.22 and p-value is 0.94. For SFR_{IR}, the KS statistic is 0.39 and p-value is 0.4. In both cases, the null hypothesis that the two samples are drawn from the same distribution cannot be rejected. Therefore, the SFR distribution of the radio-loud quasar hosts does not differ significantly from the radio-quiet population. This could mean that the presence of the jet does not have an effect on the SFR or both negative and positive feedback play a role resulting in comparable SFRs in the host galaxies of radio-loud quasars.

The role of negative and positive feedback can change depending on the evolutionary stage of the jet. Simulations show that initially the turbulence induced by the jet into the interstellar medium (ISM) causes a decrease of the SFR. Once the jet decouples from the disk, this effect weakens and the positive feedback becomes stronger (Mandal et al. 2021). The ages of the jet were previously estimated for two quasars in our sample. Momjian et al. (2008) estimated the age of J1427+3312 to be $\sim 10^3$ yr based on the typical advance speed of CSOs and the distance between the radio lobes. P172+18 was classified as a Compact Steep Spectrum (CSS) radio source (Momjian et al. 2021). Assuming a typical advance speed for such objects, the age of the jet of P172+18 is ~ 1700 yr. Both of these quasars with

very young jets have faint [CII] and FIR continuum emission and low SFRs, consistent with the expectation that negative feedback plays a more important role for younger sources. However, it is necessary to obtain the estimates of the jet age for the remaining quasars in the sample to confirm this scenario.

We note that in deriving SFRs, we assumed that [CII] and IR luminosities are only related to the star formation in the host galaxies. This is a reasonable assumption for radio-quiet quasars at $z \gtrsim 6$ (Venemans et al. 2017; Novak et al. 2019; Pensabene et al. 2021; Meyer et al. 2022; Decarli et al. 2022), but has not yet been tested for radio-loud ones. If AGN-related sources of [CII] and IR emission are significant, we are overestimating the SFRs.

In our measurements of SFR_{IR}, we assumed that the FIR continuum emission is attributed to the cold dust only. However, this is not always the case for radio-loud quasars. Rojas-Ruiz et al. (2021) shows that the FIR continuum emission of P352–15, one of the most powerful radio-loud quasars known in the early Universe (Bañados et al. 2018a), cannot be reproduced by using a MBB model only. Therefore, the synchrotron emission from the jet can contribute to the FIR continuum emission.

The [CII] emission can arise from photon-dominated regions (PDR) associated with the star formation in the host galaxy or from the X-ray dominated region (XDR) where the gas is affected by the X-ray photons from the AGN or from shocks. The X-ray radiation heats the gas and can potentially cause negative AGN feedback on star formation. One way to determine whether XDR contributes to a significant fraction of the [CII] emission is by measuring [CII]/[CI] luminosity ratio. XDR and PDR models show that CI is more abundant in XDR (e.g. Meijerink et al. 2007). The observations of [CI] and [CII] emission lines in radio-quiet quasars point to the PDR origin of their [CII] emission (Venemans et al. 2017; Novak et al. 2019; Pensabene et al. 2021; Meyer et al. 2022; Decarli et al. 2022), but the [CI] emission line has not yet been observed for any of the quasars in our sample.

Notably, the two quasars with the brightest [CII] emission in our sample are also the brightest X-ray sources known at $z \gtrsim 6$ (Medvedev et al. 2020, 2021). Their intrinsic X-ray radiation could be lower because X-ray luminosity can be enhanced by the inverse Compton scattering of the CMB photons by electrons in the jets, which is particularly important at high redshift (e.g., Ighina et al. 2021; Connor et al. 2021; Medvedev et al. 2021). Nevertheless, the observed high X-ray luminosities of these two quasars can be an indication of higher XDR contribution to the [CII] emission than in quasars with moderate or low X-ray luminosities.

In addition, [CII] can also arise from shocks produced by interactions between jets and the gas in the host galaxy (e.g., Appleton et al. 2018; Smirnova-Pinchukova et al. 2019) or in mergers, where the shocks occur due to collision of gas rich galaxies (e.g., Appleton et al. 2013; Peterson et al. 2018). All the quasars in our sample have evidence of jets. Therefore it is plausible that a fraction of the [CII] emission observed originates from shocks. In addition, J2318+3113 has been classified as a galaxy merger (Neeleman et al. 2021) and we have proposed J1429+5447 as another candidate where strong gravitational interactions might be happening (see discussion in Section 4.1).

Table 4. The IR and [CII] luminosities and SFRs of radio-loud quasars at $z \gtrsim 6$

Quasar	$\log(L_{IR}/L_\odot)$	$\log(L_{[CII]}/L_\odot)$	$\log SFR_{IR}(M_\odot yr^{-1})$	$\log SFR_{[CII]}(M_\odot yr^{-1})$
J0309+2717	13.07 ± 0.01	9.40 ± 0.03	3.07 ± 0.01	2.57 ± 0.04
J1427+3312	$11.68^{+0.11}_{-0.16}$	$8.82^{+0.06}_{-0.07}$	$1.68^{+0.11}_{-0.15}$	$1.88^{+0.07}_{-0.09}$
J1429+5447	12.92 ± 0.02	$9.55^{+0.02}_{-0.03}$	2.92 ± 0.02	2.75 ± 0.03
P172+18	$< 11.61^a$	$< 8.37^a$	$< 1.61^a$	$< 1.35^a$
J2318–3113[b]	$12.02^{+0.09}_{-0.11}$	9.20 ± 0.04	$2.02^{+0.09}_{-0.11}$	2.33 ± 0.05
P352–15	11.93 ± 0.50	$9.09^{+0.06}_{-0.08}$	1.93 ± 0.50	$2.21^{+0.08}_{-0.08}$

Notes. [a] The upper limits are at 3σ [b] The flux measurements are taken from Venemans et al. (2020). The luminosities and SFRs are recalculated following the approach in Section 4.2
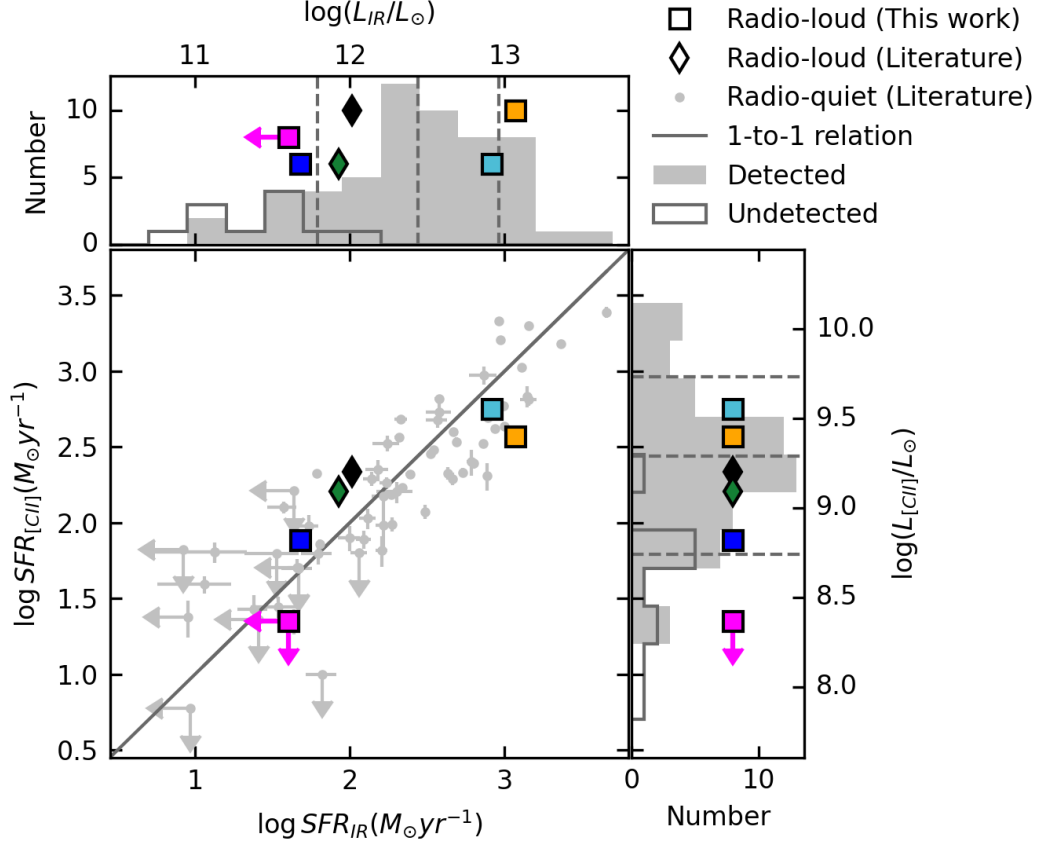
Fig. 4. The SFRs of radio-quiet (grey circles) and radio-loud (colored symbols) quasars at $z \gtrsim 6$ using [CII] and IR luminosities as SFR tracers. The radio-loud quasars from our sample are shown as squares and from the literature as thin diamonds. Colors for radio-loud quasars are the same as in Fig. 3. The solid line shows the 1-to-1 relation. The SFR (luminosity) distributions of radio-quiet quasars are shown (grey histograms). The dashed lines show the 16th, 50th and 84th percentiles of the distributions for radio-quiet quasars. References for the literature measurements are in the main text, Section 4.2.

The combination of all these effects could explain the bright [CII] emission observed in these two sources.

Our current data do not allow to determine the origin of FIR emission and [CII] line emission and it is possible that both SFR_{IR} and $SFR_{[CII]}$ are overestimated. If this is the case, the SFRs for radio-loud quasars would then all be below 64th percentile of the distribution for radio-quiet quasars (based on [CII]). The lack of highly star-forming host galaxies can be either due to stronger negative feedback from the jet or just a small number statistics.

5. Conclusions

We presented [CII] and underlying continuum observations of four (out of five known) radio-loud quasars at $z > 6$ with NOEMA. Four radio-loud quasars are robustly detected in [CII] and their underlying continuum (three from our NOEMA survey and one from previous ALMA observations), while P172+18, the highest-redshift radio-loud quasar known to date ($z = 6.8$), remained undetected.

The spectral profiles of the [CII] line differ between all three detected host galaxies in our sample. The spectral profile of J1427+3312 is best described by one Gaussian. However, the fit with two Gaussians suggests a possible presence of the broad component with FWHM$\sim 900-1400$,

which can be associated with high-velocity outflows. The SNR the current data is insufficient to make firm conclusions. J0309+2717 has a spectral profile well reproduced by a single Gaussian, similar to what is observed in radio-quiet quasars. J1429+5447 shows a clear signature of two components with widths $\mathrm{FWHM}_{broad} = 650 \pm 128$ km s^{-1} and $\mathrm{FWHM}_{narrow} = 253 \pm 38$ km s^{-1}. Based on their similarity to CO (2–1) line observed with VLA (Wang et al. 2011), we conclude that the host galaxy of J1429+5447 is likely a merger. J2318–3113 is another known merger from the literature (Neeleman et al. 2021) radio-loud quasar hosted in galaxy merger. This makes the fraction of mergers among host galaxies of radio-loud quasars $> 40\%$ at $z > 6$ only marginally higher than of radio-quiet quasars. Since our current data do not allow us to determine whether the host galaxies of the remaining three quasars are mergers, no conclusions can be made about the evolution of the merger fraction with redshift.

The [CII] and IR luminosity distributions of radio-loud quasars are comparable with that of radio-quiet quasars. If the [CII] emission and underlying continuum emission is only linked to the SFR in the host galaxy, the properties of host galaxies of radio-loud quasars are thus similar to the radio-quiet population covering the same range of SFRs. However, several other sources of [CII] and IR emission could be present in radio-loud quasars presented. The FIR flux can include contribution from the synchrotron emission the FIR flux and [CII] emission possibly originates from XDR or the shocks from interaction between the jet and the ISM. If this is the case, the SFRs of the host galaxies are overestimated and can be lower than in radio-quiet quasars. This would imply a negative feedback from the jet. Verifying this hypothesis requires more measurements of the rest-frame FIR continuum and radio slope at high frequencies and multi-line data.

References

Andika, I. T., Jahnke, K., Onoue, M., et al. 2020, ApJ, 903, 34
Appleton, P. N., Diaz-Santos, T., Fadda, D., et al. 2018, ApJ, 869, 61
Appleton, P. N., Guillard, P., Boulanger, F., et al. 2013, ApJ, 777, 66
Bañados, E., Carilli, C., Walter, F., et al. 2018a, ApJ, 861, L14
Bañados, E., Decarli, R., Walter, F., et al. 2015a, ApJ, 805, L8
Bañados, E., Mazzucchelli, C., Momjian, E., et al. 2021, ApJ, 909, 80
Bañados, E., Venemans, B. P., Mazzucchelli, C., et al. 2018b, Nature, 553, 473
Bañados, E., Venemans, B. P., Morganson, E., et al. 2015b, ApJ, 804, 118
Beelen, A., Cox, P., Benford, D. J., et al. 2006, ApJ, 642, 694
Belladitta, S., Moretti, A., Caccianiga, A., et al. 2020, A&A, 635, L7
Bischetti, M., Maiolino, R., Carniani, S., et al. 2019, A&A, 630, A59
Boogaard, L., Meyer, R. A., & Novak, M. 2021, Interferopy: analysing datacubes from radio-to-submm observations
Carilli, C. L. & Walter, F. 2013, ARA&A, 51, 105
Chabrier, G. 2003, Publications of the Astronomical Society of the Pacific, 115, 763
Chiaberge, M., Gilli, R., Lotz, J. M., & Norman, C. 2015, ApJ, 806, 147
Cicone, C., Maiolino, R., Gallerani, S., et al. 2015, A&A, 574, A14
Condon, J. J., Cotton, W. D., Greisen, E. W., et al. 1998, AJ, 115, 1693
Connor, T., Bañados, E., Stern, D., et al. 2021, ApJ, 911, 120
Conway, J. E. 2002, New A Rev., 46, 263
da Cunha, E., Groves, B., Walter, F., et al. 2013, ApJ, 766, 13
De Looze, I., Cormier, D., Lebouteiller, V., et al. 2014, A&A, 568, A62
Decarli, R., Pensabene, A., Venemans, B., et al. 2022, arXiv e-prints, arXiv:2203.03658
Decarli, R., Walter, F., Venemans, B. P., et al. 2017, Nature, 545, 457
Decarli, R., Walter, F., Venemans, B. P., et al. 2018, ApJ, 854, 97
Di Matteo, T., Springel, V., & Hernquist, L. 2005, Nature, 433, 604
Dunne, L., Eales, S. A., & Edmunds, M. G. 2003, MNRAS, 341, 589
Eilers, A.-C., Hennawi, J. F., Decarli, R., et al. 2020, ApJ, 900, 37
Frey, S., Gurvits, L. I., Paragi, Z., & É. Gabányi, K. 2008, A&A, 484, L39
Frey, S., Paragi, Z., Gurvits, L. I., Gábányi, K. É., & Cseh, D. 2011, A&A, 531, L5
Gloudemans, A. J., Duncan, K. J., Röttgering, H. J. A., et al. 2021, A&A, 656, A137
Högbom, J. A. 1974, A&AS, 15, 417
Ighina, L., Belladitta, S., Caccianiga, A., et al. 2021, arXiv e-prints, arXiv:2101.11371
Ighina, L., Moretti, A., Tavecchio, F., et al. 2022, A&A, 659, A93
Inayoshi, K., Visbal, E., & Haiman, Z. 2020, ARA&A, 58, 27
Intema, H. T., Jagannathan, P., Mooley, K. P., & Frail, D. A. 2017, A&A, 598, A78
Izumi, T., Onoue, M., Matsuoka, Y., et al. 2019, PASJ, 71, 111
Izumi, T., Onoue, M., Shirakata, H., et al. 2018, PASJ, 70, 36
Jolley, E. J. D. & Kuncic, Z. 2008, MNRAS, 386, 989
Jorsater, S. & van Moorsel, G. A. 1995, AJ, 110, 2037
Kass, R. E. & Raftery, A. E. 1995, Journal of the American Statistical Association, 90, 773
Kellermann, K. I., Sramek, R., Schmidt, M., Shaffer, D. B., & Green, R. 1989, AJ, 98, 1195
Kennicutt, Robert C., J. 1998, ApJ, 498, 541
Liu, Y., Wang, R., Momjian, E., et al. 2021, ApJ, 908, 124
Maiolino, R., Cox, P., Caselli, P., et al. 2005, A&A, 440, L51
Maiolino, R., Gallerani, S., Neri, R., et al. 2012, MNRAS, 425, L66
Mandal, A., Mukherjee, D., Federrath, C., et al. 2021, MNRAS[arXiv:2109.13654]
McGreer, I. D., Becker, R. H., Helfand, D. J., & White, R. L. 2006, ApJ, 652, 157
Medvedev, P., Gilfanov, M., Sazonov, S., Schartel, N., & Sunyaev, R. 2021, MNRAS, 504, 576
Medvedev, P., Sazonov, S., Gilfanov, M., et al. 2020, MNRAS, 497, 1842
Meijerink, R., Spaans, M., & Israel, F. P. 2007, A&A, 461, 793
Meyer, R. A., Walter, F., Cicone, C., et al. 2022, arXiv e-prints, arXiv:2201.08143
Momjian, E., Bañados, E., Carilli, C. L., Walter, F., & Mazzucchelli, C. 2021, AJ, 161, 207
Momjian, E., Carilli, C. L., & McGreer, I. D. 2008, AJ, 136, 344
Mufakharov, T., Mikhailov, A., Sotnikova, Y., et al. 2020, arXiv e-prints, arXiv:2011.12072
Neeleman, M., Novak, M., Venemans, B. P., et al. 2021, ApJ, 911, 141
Novak, M., Bañados, E., Decarli, R., et al. 2019, ApJ, 881, 63
Novak, M., Venemans, B. P., Walter, F., et al. 2020, ApJ, 904, 131
Pensabene, A., Decarli, R., Bañados, E., et al. 2021, A&A, 652, A66
Peterson, B. W., Appleton, P. N., Bitsakis, T., et al. 2018, ApJ, 855, 141
Rojas-Ruiz, S., Bañados, E., Neeleman, M., et al. 2021, ApJ, 920, 150
Shen, Y., Wu, J., Jiang, L., et al. 2019, ApJ, 873, 35
Shimwell, T. W., Tasse, C., Hardcastle, M. J., et al. 2019, A&A, 622, A1
Silk, J. 2013, ApJ, 772, 112
Smirnova-Pinchukova, I., Husemann, B., Busch, G., et al. 2019, A&A, 626, L3
Spingola, C., Dallacasa, D., Belladitta, S., et al. 2020, A&A, 643, L12
Venemans, B. P., McMahon, R. G., Walter, F., et al. 2012, ApJ, 751, L25
Venemans, B. P., Walter, F., Decarli, R., et al. 2017, ApJ, 851, L8
Venemans, B. P., Walter, F., Neeleman, M., et al. 2020, ApJ, 904, 130
Venemans, B. P., Walter, F., Zschaechner, L., et al. 2016, ApJ, 816, 37
Villar Martín, M., Emonts, B., Humphrey, A., Cabrera Lavers, A., & Binette, L. 2014, MNRAS, 440, 3202
Volonteri, M., Habouzit, M., & Colpi, M. 2021, arXiv e-prints, arXiv:2110.10175
Volonteri, M., Silk, J., & Dubus, G. 2015, ApJ, 804, 148
Walter, F. & Brinks, E. 1999, AJ, 118, 273
Walter, F., Riechers, D., Cox, P., et al. 2009, Nature, 457, 699
Wang, F., Yang, J., Fan, X., et al. 2021, ApJ, 907, L1
Wang, R., Wagg, J., Carilli, C. L., et al. 2013, ApJ, 773, 44
Wang, R., Wagg, J., Carilli, C. L., et al. 2011, ApJ, 739, L34
Wang, R., Wu, X.-B., Neri, R., et al. 2016, ApJ, 830, 53
Willott, C. J., Bergeron, J., & Omont, A. 2015, ApJ, 801, 123
Willott, C. J., Bergeron, J., & Omont, A. 2017, ApJ, 850, 108
Willott, C. J., Delorme, P., Reylé, C., et al. 2010, AJ, 139, 906
Willott, C. J., Omont, A., & Bergeron, J. 2013, ApJ, 770, 13
Yang, J., Venemans, B., Wang, F., et al. 2019, ApJ, 880, 153
Yang, J., Wang, F., Fan, X., et al. 2020, ApJ, 897, L14